Evaluation of Postmortem Changes in Tissue Structure in the Bottlenose Dolphin (*Tursiops truncatus*)

MEGAN F. MCKENNA,[1]* JEREMY A. GOLDBOGEN,[2] JUDY ST. LEGER,[3]
JOHN A. HILDEBRAND,[1] AND TED W. CRANFORD[4]

[1]Scripps Institution of Oceanography, University of California, San Diego, La Jolla,
California
[2]Department of Zoology, University of British Columbia, Vancouver, British Columbia,
Canada
[3]Seaworld, San Diego, San Diego, California
[4]San Diego State University, San Diego, California

ABSTRACT

Postmortem changes in geometry, density, and sound speed within organs and tissues (melon, bone, blubber, and mandibular fat) of the dolphin head were evaluated using computed tomography (CT) scans of live and postmortem bottlenose dolphins (*Tursiops truncatus*). Specimens were classified into three different treatment groups: live, recently dead, and frozen followed by thawing. Organs and tissues in similar anatomical regions of the head were compared in CT scans of the specimens to identify postmortem changes in morphology. In addition, comparisons of Hounsfield units in the CT scans were used to evaluate postmortem changes in the density of melon, bone, blubber, and mandibular fat. Sound speed measurements from melon, blubber, connective tissue, and muscle were collected from fresh and frozen samples in the same specimen to evaluate effects due to freezing and thawing process on sound speed measurements. Similar results in tissue and organ geometry, density, and sound speed measurements suggested that postmortem material is a reliable approximation for live melon, bone, blubber, muscle, connective tissue, and mandibular fat. These results have implications for examining viscoelastic properties and the accuracy of simulating sound transmission in postmortem material. Anat Rec, 290:1023–1032, 2007. © 2007 Wiley-Liss, Inc.

Key words: x-ray; computed tomography; postmortem; *Tursiops truncatus*; sound speed; melon; Hounsfield unit; density

The internal structure of complex forms can be studied using X-ray computed tomography (CT). Like most remote imaging techniques, one of the main benefits is that geometric relationships between structures are maintained in the images (Cranford, 1996; Marcucci et al., 2001; Marino et al., 2004; Summers et al., 2004). Furthermore, models of biological systems can be built using accurate morphological descriptions extracted from CT scans and tissue property data gathered from CT images and other techniques (Aroyan et al., 1992; Richardson et al., 1995; Terheyden et al., 2000; Aroyan, 2001; Soldevilla et al., 2005a).

Capturing CT data from live animals is common in humans and a variety of small terrestrial mammals for clinical studies; however, obvious challenges arise when attempting to scan live aquatic mammals; only one study to date has successfully overcome these challenges
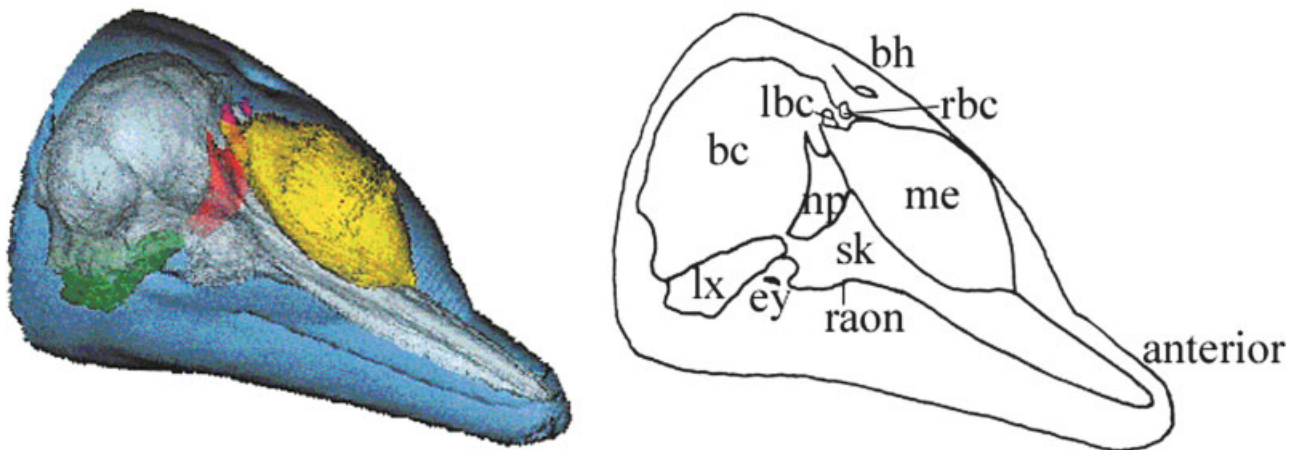
Fig. 1. Three-dimensional computed tomography image of the sound production anatomy in the bottlenose dolphin head. sk, skull; np, nasal passages; lx, larynx; rbc, right bursae complex; lbc, left bursae complex; me, melon; bc, brain case; ey, eye; bl, blowhole; raon, right anterior orbital notch.

(Houser et al., 2004). Remote imaging techniques are usually performed on recently dead, frozen, and/or thawed specimens (Cranford, 1996; Maisano et al., 2002; Carpenter et al., 2004). Stranded postmortem marine mammals are often transported to laboratories and sometimes frozen until CT scanning, experiments, or observations can be made. This report is the first study to examine the accuracy of using postmortem toothed whales as representation of live tissue structure and physical properties (density and sound speed).

We are particularly interested in looking at postmortem changes in the acoustic anatomy of odontocetes (toothed whales). The anatomy of sound production/propagation (Fig. 1) is a well investigated topic in odontocetes (Mead, 1975; Heyning, 1989; Cranford, 1992, 1996; Au, 1993; Cranford et al., 1997, 2000). It is generally accepted that click generation begins by action of the palatopharyngeal muscle complex, as it forces the larynx up into the inferior bony nares and pressurizes the air in the bony nasal passages. The pressurized air passes through lips formed by a narrow slit in the spiracular cavity, causing vibrations in adjacent ellipsoid fat bodies. These vibrations are reflected forward by the skull and air sacs functioning as acoustic mirrors. The sound vibrations propagate through the melon anteriorly and emerge into the environment as a click. The melon is a fat and connective tissue organ that functions to focus sound and decrease acoustic attenuation at the tissue–water boundary (Cranford and Amundin, 2004).

The geometry and elastic properties within the structures of the forehead will determine the sound propagation and reception pathways. CT provides a means to characterize the geometry and density topography within these organs and tissues (Cranford, 1996; McKenna, 2005; Au et al., 2006). When these data are combined with sound speed measurements and finite element tools, acoustic simulations of the organs are possible (Soldevilla et al., 2005a).

The present study compares CT scans of postmortem and live bottlenose dolphin heads in an effort to understand postmortem effects on tissue and organ structure and physical properties, specifically density. Changes in

sound speed are also measured in one specimen before and after the freezing and thawing process. The resulting data will help identify the limitations of using postmortem material to represent living biological systems.

MATERIALS AND METHODS

For the morphological and density analyses, the heads of four bottlenose dolphins (*Tursiops truncatus*) were compared. Previous studies show that there is significant cephalic morphological differences between species of odontocetes (Cranford, 1996; McKenna, 2005), therefore, we choose to analyze four animals of the same species and of similar age. The specimens were all adult bottlenose dolphins of similar age and size (Table 1). The specimens were divided into three treatment groups: one living (LIVE), one recently dead (FRESH), and two frozen then thawed (THAWED). A live trained dolphin (LIVE) in the Navy Marine Mammal Program was CT scanned for a previous study (Houser et al., 2004), and the resulting CT data were made available for this study. The FRESH specimen was an adult female from a captive collection that died on 24 April 2004 from a gastrointestinal condition. The heads of the THAWED specimens (THAWED A and THAWED B) were obtained from the Navy Marine Mammal Program. The sound speed measurements were made on the FRESH specimen, one of the four dolphins mentioned above.

Data Acquisition

X-ray computed tomography data were collected as a series of digital images, thin cross-sections of the specimen known as serial tomograms or scans. Each scan was composed of a matrix of values (CT numbers) expressing a measure of linear attenuation of X-rays through the material at a specific geometric location within the specimen. The information was then stored in a digital format specific to each scanner.

After the death of the animals, the heads of specimens THAWED A and THAWED B were separated from the

TABLE 1. Specimen life history information

Group	Specimen ID	Date of death	Location	Age	Sex	Body length (cm)	Weight (kg)	Date of CT scan
THAWED A	Tutr790	3/11/1985	San Diego, CA	Adult	Male	239	136	6/12/1986
THAWED B	Tutr567	5/26/1987	San Diego, CA	Adult	Male	238	153	2/8/1988
FRESH	Tutr2082	4/24/2004	San Diego, CA	Adult	Female	278	162	4/24/2004
LIVE	Tutr21030	Alive	San Diego, CA	Adult	Female	222	122	4/3/2002

body at the occipital condyles during the necropsy. They were placed in plastic bags and stored at 4°C for 1 year. THAWED A head was put in the freezer 4–6 hr after death; however, THAWED B was left out longer during the necropsy (6–8 hr). In preparation for CT scanning, the heads were thawed in a water bath at room temperature for approximately 36 hr to promote rapid and even thawing of the specimens. THAWED A and B were scanned using a General Electric 9800 X-ray CT scanner with an X-ray tube voltage of 140 kV (kilovolts) and 70 and 120 mAs (millamp seconds) at the University of California, San Francisco, in 1989 and 1986, respectively. Serial tomograms were collected continuously from the tip of the rostrum to the occipital condyles without intervening spaces. The slice thickness varied depending on the interest in a particular region. From the tip of the rostrum to the anterior border of the nasal passages, the slice thickness was 5 mm. In the adjacent region, the nasal air sacs and the sound generation complexes, the X-ray beam was narrowed to a thickness of 1.5 mm to record the greatest detail. The scan thickness increased to 3 mm over the posterior portion of the head. The 16-bit signed image data were stored as proprietary (GE9800) file format until further processing.

The FRESH specimen was scanned on a GE Light-Speed Plus helical scanner at Thornton Hospital, University of California, San Diego on 24 April 2004 (X-ray source: 120 kV and 260 mAs). The scanning commenced 4 hr after death. Axial scans were collected continuously every 2.5 mm, and the entire head was scanned. The 16-bit signed image data was stored as DICOM file format until processing.

Details of the scanning protocol for the LIVE dolphin can be found in Houser et al. (2004). In brief, X-ray CT was performed using an electron beam Imatron scanner at vital images in La Jolla, California on March 3, 2002. X-ray data were acquired helically with a source voltage of 130 kV and 600 mAs. Axial scans were collected continuously every 2.5 mm, and the entire head was scanned. Image data were saved in DICOM format.

Because we decided to control for species differences, our ability to control the specifics of the CT scanner parameters was compromised. The four specimens were scanned on three different scanners, with different voltage and current settings, and slice thickness. Potentially heterogeneous scanner data were used in this analysis because of the scarcity of new specimens of the same species and size and expenses associated with CT scanning.

Image Processing

Hounsfield (H) values are the units used in medical CT imaging to describe the amount of X-ray attenuation within each "voxel" (volume element of known dimension) in the three-dimensional image. The H units are a calibrated measure of electron density, which is equivalent to the change in density of one cubic centimeter of water one degree centigrade at standard temperature and pressure. It is possible to express the H values in terms of physical density based on a previous study that established a calibration curve of physical density vs. CT number within the normal constraints of variation and drift (Mull, 1984). The H values are arranged on a scale from −1,024H unit to +3,071H unit, calibrated so that −1,024H unit is the attenuation produced by air and 0H unit is the attenuation produced by water (Robb, 1999).

Image formats from the CT scanners in this study included both DICOM and GE9800. The DICOM images from the LIVE and FRESH specimens contain information on two fields (rescale slope and rescale intercept) that convert each voxel in the image to a Hounsfield scale (−1,024 to +3,071). The DICOM standard always rescales back to the actual H values, making the volumes directly comparable. The GE9800 images were collected before the DICOM standard existed. Consequently, serial images from THAWED A and THAWED B were adjusted to match the DICOM values. The GE9800 scanner added 1,024 to each voxel value. To rescale the images back to their original H values, 1,024 was subtracted from all values in the GE9800 images. There is variation in the calibration of each scanner, potentially introducing some noise to the actual H values.

Data acquired for all specimens were processed using Analyze 5.0 and 6.0, created by the Biomedical Imaging Resource at Mayo Clinic (Robb and Barillot, 1989; Robb et al., 1989; Robb, 1999). The individual CT scan slices were compiled and converted to AVW formats (a native Analyze format). The AVW format is a volumetric file and composed of calibrated H units for each voxel in the image. To visualize and analyze volumes of uniform voxel dimensions, the voxels in each specimen were interpolated to 1.5 mm^3.

Morphological Structure

The morphological structures of the forehead region were compared between the LIVE, FRESH, and THAWED specimens to evaluate effects of death and/or freezing on tissue structure. The H values at similar locations within the forehead of each specimen were compared using "line profiling," an image processing technique. Line profiling is accomplished by highlighting a linear set of pixels in a two-dimensional image or "slice." The H values of the pixels along the line are plotted against location within the head.

To make the line profiles comparable, the locations for the line profiles were standardized by reference to

an anatomic landmark: a transverse slice through the posterior border of the antorbital notch (Figs. 1, 3). The region was of particular interest because it contained the melon. To characterize the structure of the melon, three different locations were analyzed: dorsal, middle, and ventral. Line profiles were traced across the width of each specimen at three locations in the melon, designated as UPPER, MIDDLE, and LOWER, as shown in Figure 3.

Specimens differed slightly in size, so the profiles were aligned at the mid-sagittal plane of each specimen. The resulting figure allows visual comparison of internal melon structure based on changes in H values across the same anatomic location. In the same line profiles, the structure of the melon was also analyzed for postmortem changes in geometry. To quantify melon structure, the slopes of the left and right side were calculated and compared across specimens.

To determine the degree of correlation between the H values in the head and melon profiles of the postmortem specimens compared with the live specimen, a linear regression was performed for all three profile analyses (UPPER, MIDDLE, and LOWER); a standard statistical package was used (SPSS, 2000). The right and left sides of the profiles were analyzed separately, because the slopes of the sides differed in all profiles.

Hounsfield Units

In addition to morphological comparisons, changes in density of various tissues and organs were analyzed. The maximum, minimum, and average H values were recorded for a region of the segmented structures within the heads: the melon, cranium, muscle, blubber, and mandibular fat (Fig. 1). Each segmented area contained several adjacent slices, and the variation within each specimen was analyzed. The mean H values were calculated for each tissue and averaged within each specimen. The means were then compared among the four specimens.

To segment the melon and bones from the surrounding tissue, a specific range of H values was defined. The H values of each voxel in the volume were mapped onto a gray or color scale, thus allowing visualization of differences in tissue density based on gray scale intensity or color differences (Fig. 2). The specific ranges of H values for bone were as follows: THAWED A, 1551.7 to 152; THAWED B, 1542.3 to 147; FRESH, 1701.6 to 111.3; and LIVE, 1504 to 220.1. The bone boundaries were compared to an actual skull to determine accuracy. The specific ranges of H values for melon were as follows: THAWED A, -32.6 to -127, THAWED B, -60.2 to -127.6; FRESH, -63.9 to -123.8; and LIVE, -51.1 to -140.2. The melon boundaries were determined based on a 10 H value or greater change at adjacent points in the MIDDLE profiles.

The regions of muscle, blubber, and mandibular fat were sampled in the same location in the head of all specimens. The boundaries in these tissues were drawn using an imaging processing tool: a square of the same dimensions (10 mm $\times$ 10 mm $\times$ 1.5 mm) was placed in the same anatomic location in each specimen.

To determine whether there were significant differences in the H values of the postmortem specimens compared with the live specimen for the melon and bones,

an analysis of variance (ANOVA) was performed; a standard statistical package was used (SPSS, 2000). The blubber, muscle, and connective tissue were not compared statistically because the of the low sample size from each specimen.

Sound Speed

The change in sound speed, as a function of time from death, was measured in the FRESH (recently dead) specimen in different tissues and organs to investigate effects of the freezing and thawing process. After the FRESH specimen was CT scanned (approximately 4 hr from death), the head was cut mid-sagittally (longitudinally) with a band saw into left and right halves. The left half was wrapped tightly in plastic wrap and frozen at $-14°$C; the right half was prepared for sound speed measurements. Cubes of tissue approximately 3–6 cm^3 were cut from the exposed mid-sagittal surface (Fig. 2).

The speed of sound through each tissue sample was measured using a Krautkramer Branson USD10 Ultrasonic Digital Flaw Detector and two Krautkramer Branson longitudinal acoustic transducers (Alpha series, 10 MHz, 0.25 mm) attached to Mitutoyo digital calipers (model no. CD-8″CS; Soldevilla et al., 2005b). Before measuring the samples, the velocimeter was calibrated using room-temperature (22.5°C) distilled water, assuming a sound speed of 1,490 m/sec (Chen and Millero, 1977). Measurements were collected at room temperature (22.5°C). The Krautkramer velocimeter produced 10 MHz broadband pulses that were directed into the face of one side of each tissue cube and received at the other end yielding a transmission time. Calipers were used to determine the sample thickness, and sound speed was calculated by dividing the thickness by the transmission time.

Sound speed was calculated for each tissue sample by averaging three trials along each axis (anterior–posterior, lateral, and dorsal–ventral), assuming no significant difference with orientation (Soldevilla et al., 2005b). The first set of sound speed measurements were collected 7.5 hr after death. The measurements were repeated at 27, 100, 149, and 172 hr after death. Between sound speed measurements, the samples were stored in zip-lock bags at room temperature (22.5°C).

The frozen half of the head was removed from the freezer after 17 days and thawed at room temperature for 12 hr before sampling. Cubes of tissue, at approximately the same anatomic locations and of the same size as the fresh samples, were removed from the left half of the head (Fig. 2). Each sample was measured using the same techniques described for the previous paragraph. It was assumed that time from death stopped during the freezing stage and resumed when the specimen was thawed. Sound speed was measured in these samples at 21, 46, 69, 93, and 120 hr after thawing.

The seven tissue samples were sorted into three groups: (1) melon (posterior melon core, middle melon core, anterior melon core, and anterior melon shell), (2) connective tissue (connective tissue and blubber), and (3) muscle (gular musculature). Although there were some differences in sound speed within the pooled groups, the difference was found to be less than the differences between the groups. All data were statistically
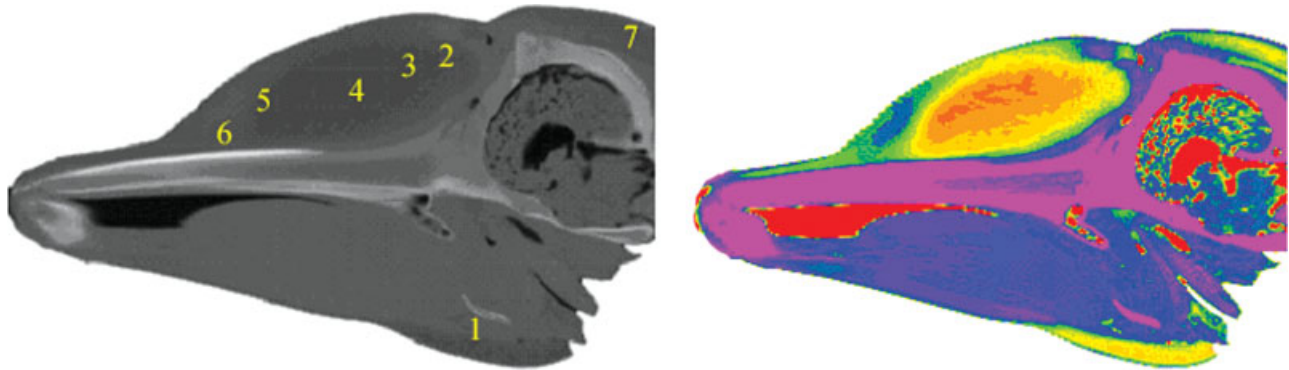
Fig. 2. Enhanced visualization of the computed tomography images displayed on *Tursiops truncatus* (Tutr790). In the black and white image, all H values (−1,024 to +2,466) have been mapped onto a gray scale map. In the color image, the adjusted scale of H values is displayed (−184 to +157) with a color map. Notice the enhanced depiction of bone (white) in the black and white image and the highlighted distinction of boundaries in soft tissue in the color image. The locations of tissue samples used for sound speed measurements are labeled: 1, hyoid muscle; 2, posterior melon core; 3, middle melon core; 4, anterior melon core; 5, anterior melon shell; 6, connective tissue; and 7, blubber.
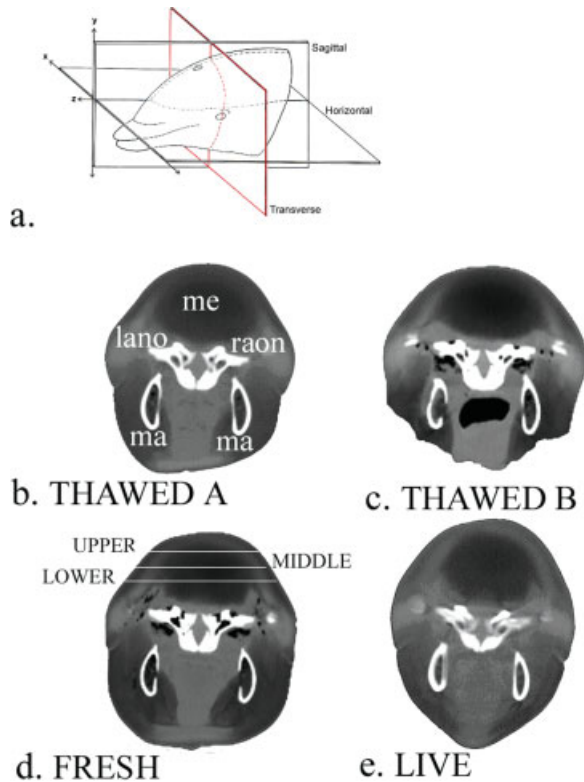

Fig. 3. Location and transverse scans at the antorbital notch in all *Tursiops* specimens. **a:** Location and orientation of transverse scan. **b:** Thawed specimen (Tutr790). Labeled structures: me, melon; ma, mandibles; lano, left anterior orbital notch; raon, right anterior orbital notch. **c:** Thawed specimen (Tutr567). **d:** Fresh specimen (Tutr2084). The lines show the location of the three profiles in the melon analyzed. **e:** Live specimen (Tutr20831). d,e: The gray scale images are individually adjusted using window-level settings to highlight the bone (white) and soft tissue structures (grays).

Fig. 4. Density change across the LOWER profile of all *Tursiops* specimens. The *y*-axis represents the change in Hounsfield values plotted over a specified distance across the section of the animal (mm) on the *x*-axis. Drop in density at the blubber layer surrounding the heads (a), connective tissue invades the sides of the melon (b), and the melon (c).

analyzed for normality of distribution and equal variance. The sound speed results for both the fresh and frozen tissue types were tested separately for significant differen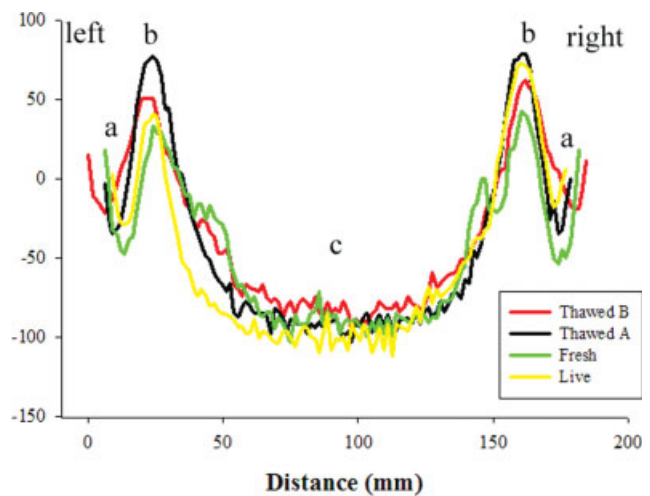ces as a result of time lapsed from death using an ANOVA and Bonferroni post hoc test. To identify significant differences between fresh and thawed samples, a two-tailed *t*-test was used ($P = 0.05$) if the distribution for each tissue type was normal. The Wilcoxon test was used for the same purpose if the distribution was not normal.

RESULTS
Morphological Structure

A slight slumping forward of the dorsal and ventral regions in the superficial soft tissues of the forehead in the postmortem specimens most likely resulted from disarticulating the head from the body (Fig. 3). Nevertheless, the structure of the melon and surrounding tissues in the four specimens were similar in the three line profiles analyzed.

TABLE 2. Results of the regression analyses (r² values) for head and melon profiles

	UPPER		MIDDLE		LOWER	
	Left	Right	Left	Right	Left	Right
Head profile						
LIVE/ THAWED A	0.905	0.943	0.618	0.790	0.655	0.402
LIVE/ THAWED B	0.838	0.879	0.773	0.782	0.874	0.312
LIVE/FRESH	0.775	0.660	0.706	0.551	0.728	0.636
Melon profile						
LIVE/ THAWED A	0.922	0.855	0.925	0.936	0.889	0.717
LIVE/ THAWED B	0.952	0.922	0.926	0.944	0.829	0.804
LIVE/FRESH	0.923	0.853	0.888	0.831	0.799	0.465

TABLE 3. Quantitative comparisons of melon morphology

Profile	THAWED A	THAWED B	FRESH	LIVE
UPPER				
Melon width (mm)	124.5	108.5	115.5	97.5
Left slope	−1.3	−1.3	−1.1	−1.6
Right slope	1.9	2.1	1	1.7
MIDDLE				
Melon width (mm)	111	111	106.5	127.5
Left slope	−1.6	−1.6	−1.2	−1.7
Right slope	1.8	1.9	2.1	1.4
LOWER				
Melon width (mm)	108	108	102	117
Left slope	−1.3	−1	−1.2	−1.1
Right slope	1.5	1.6	1.9	2.25

Comparisons between the LOWER profiles in each specimen revealed a similar drop in density at the blubber layer surrounding the heads, represented by the low values on the right and left sides of each profile (denoted by "a" in Fig. 4). Beneath the skin and blubber layer, a connective tissue layer borders the lateral sides of the melon, represented by the sharp peaks of higher density (denoted by "b" in Fig. 4). The low density "valley" in the center of all profiles is the melon (denoted by "c" in Fig. 4). In the regression analysis, comparing the LIVE to the three postmortem groups, the H values were highly correlated (Table 2). The morphology within the melon was also highly conserved across all specimens. The structure of the right side of the melon had a steeper slope or a more rapid drop in H values on the outer boundary compared with the left side of the melon in all specimens (Table 3).

In all four specimens, the MIDDLE line profile shows a decrease in maximum H value on the lateral sides of the melon compared with the LOWER profiles, represented by a shallower gradient at the blubber layer and the peaks at the connective tissue layer have lower H values. In the low density region of the profile, representing the melon core, the H values are less than the values in the LOWER profiles by approximately 10 H, indicating a lower density core at the center of the melon. Similarly, the low density melon core has steeper slopes on the right and left sides compared with the UPPER profiles. The results of the melon structure in the LIVE specimen differed slightly from this pattern in that the right side melon slope was only slightly steeper than the left. The overall similarities of H values in the FRESH and THAWED versus the LIVE are reflected in the results of the regression analysis of the profiles (Table 2). The internal structure of the melon was very similar across all specimens (Tables 2, 3).

A similar geometry of the four heads can be seen in the UPPER line profiles (Table 2). The connective tissue layer is absent in the UPPER line profile; instead, the blubber grades directly into the melon. Although the lower density core of the melon is still present, the difference of the slopes on the right and left side of the melon is less apparent in the UPPER line profiles compared with the MIDDLE and LOWER (Table 3).

Hounsfield Units

The differences between the mean H values for bone, melon, muscle, blubber, and mandible fat across the treatment groups were small. No statistically significant differences were found in the mean H values of the melon and bone when compared across the four treatment groups, but some interesting trends were apparent and worth mentioning.

The largest differences in the mean H value were found in bone. The mean H value was the highest (most dense) in the FRESH specimen, and most similar to the LIVE (Fig. 5a). For the melon samples, the LIVE specimen had the lowest mean H value (least dense), which was most similar to the FRESH specimen (Fig. 5b).

For the subsample of muscle, the mean H value was most similar between the FRESH and LIVE specimen. The H values for the blubber differed the most between THAWED specimens (14 H) and most similar in between the LIVE and FRESH. The largest difference in mandibular fat H values was between the FRESH and the LIVE (30 H).

Sound Speed

No statistically significant change was found in sound speed measurements during the time frame monitored within all fresh samples and all thawed tissue samples, however, certain patterns are apparent and worth mentioning. One pattern present in all anatomic regions analyzed was that, after 24 hr, there was a noticeable change in sound speed, then the measurements remained relatively constant until 120 hr, after which small changes in sound speed were observed. Within the melon, sound speed measurements increased as a function of time after death and then remained relatively constant until 120 hr from death; this finding was apparent in both the fresh and thawed halves of the head. The blubber samples showed the most variation between the fresh and thawed samples. The fresh and thawed muscle samples dropped in sound speed after 80 hr. The connective tissue remained fairly constant in both the fresh and thawed samples until 100 hr after death.

Because no significant difference ($P = 0.001$) was found in the sound speeds in the time frame analyzed, samples from all the times were pooled and included in
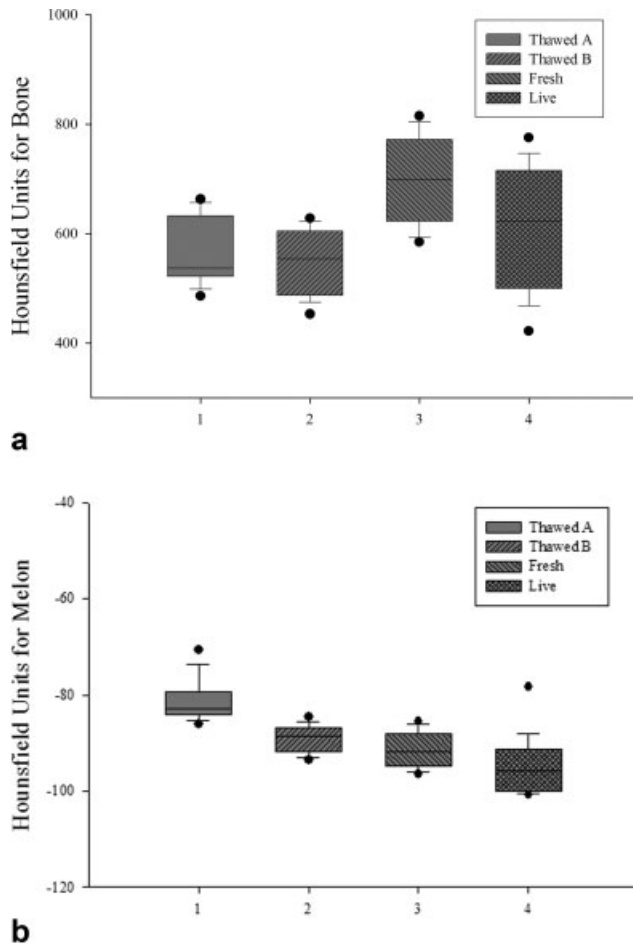
a

b

Fig. 5. **a,b:** Box plots comparing Hounsfield (H) values for bone (a) and melon (b) in all *Tursiops* specimens. (a) bone ($P = 0.115$). (b) melon ($P = 0.565$). The data in the bars are the mean H values from representative scans at the same anatomical landmarks (between the supraorbital process and a spot along the rostrum for the melon). The center vertical line marks the median of the each group. The box edges are at the 24th and 75th percentiles, and the whiskers are at the 95th and 5th percentiles. The dots represent the outliers.

the comparison between fresh and thawed samples to evaluate the effects of the freezing and thawing process on postmortem tissues and organs. No statistical differences were found between the fresh and thawed groups for all anatomic regions ($P > 0.05$: melon, 0.729; connective tissue, 0.158; muscle, 0.239; Fig. 6), suggesting that there is minimal effect on the tissue sound speed properties as a result of the freezing and thawing process.

DISCUSSION

This study demonstrates that X-ray computed tomography on postmortem material can be used to capture intricate in situ morphology without sacrificing structural integrity, corroborating previous studies investigating postmortem material (Stern and Webb, 1993; Estes et al., 1998; Schroeder, 2001). We believe that the significance of the study is that the two independent analyses
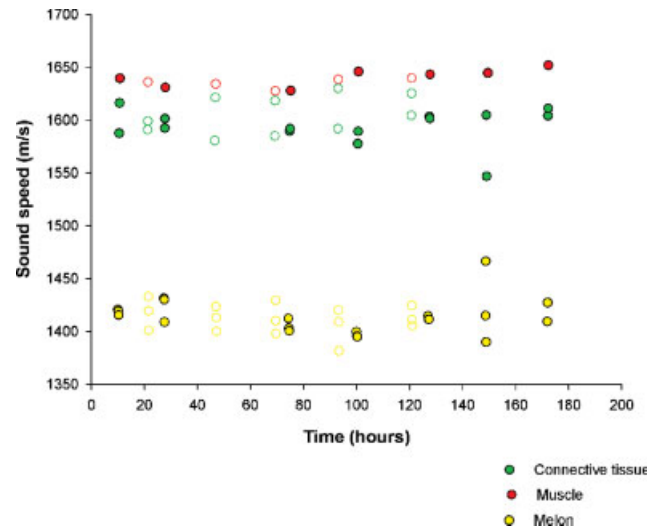

Fig. 6. The change in sound speeds for three tissue types: muscle (red), blubber (green), melon (blue). The solid circles represent measurements taken X hr from death. The open circles represent measurements taken after the specimen was frozen and thawed. Zero represents time of death. For the thawed samples, we assumed that time stopped while the specimen was frozen and started again after the thawing process. Melon $P = 0.729$; connective tissue $P = 0.158$; muscle $P = 0.239$.

(Hounsfield and morphological comparisons) showed little difference between live and postmortem biological material. In fact, the internal morphological structures were highly correlated. Based on these findings, accurate descriptions or models of internal structures and their geometry are possible from postmortem animals, with a general recommendation of CT scanning as soon after death or thawing as possible.

The comparisons of forehead and melon structure between the CT scans of THAWED and FRESH versus the LIVE specimen showed similar anatomic organization, although some external deformities were introduced by the disarticulation of the head from the body. THAWED B showed the greatest degree of external deformation (Fig. 3). The degree of deformation may be correlated with the length of time from death before placement in the freezer; THAWED B was put in the freezer 6–8 hr from death. Freezing the head immediately after disarticulation is important for maintaining the least disturbed external structure. We assume that similar external deformation as we found in THAWED B would be apparent if the CT scan of a FRESH specimen was not performed less than 6 hr after disarticulation from the body; however, additional specimen comparisons are needed to make specific time frame recommendations.

The structure and geometry of deeper anatomic structures remained intact in both the THAWED and FRESH specimens, when the CT images were compared with a scan of a LIVE animal. This study demonstrated the strong correlation between line profiles through both the forehead and melon (Table 2). This study did not determine a time from death when significant deformation can be observed in internal structures, but to observe structural integrity in the internal tissues, CT scanning

or freezing should happen within 10 hr from death based on the maximum amount of time our samples were left before scanning. However, additional specimens are needed to make any specific recommendation.

Comparisons of H values within different tissue groups (bone, melon, blubber, mandibular fat) did vary slightly, suggesting postmortem effects on tissue properties, namely density. However, we did not control for potential differences in scanner parameters, and it is difficult to determine whether the changes were related to actually postmortem changes or difference in scanner settings. The importance of these findings is that the difference in the H values is small, suggesting that postmortem changes and/or scanner effects are minimal.

The largest variations in the H units were found in the bone, both within each specimen and across treatment groups. A possible explanation for this difference is related to the composition and structure of odontocete bones. The density of the odontocete skull varies with specific bones and regions, and in general, the bones contain a significant amount of fat molecules (Rommel, 1990). Because of this matrix of material, the variation measured in this study might reflect the sensitivity of H unit measurements.

Melon, blubber, muscle, and mandibular fat are more homogenous materials and the mean H values showed a lesser degree of discrepancy among the three treatment groups (LIVE, FRESH, and THAWED). The differences between the mean melon, blubber, muscle, and mandibular fat H values were within the standard deviations of a previous study examining physical properties of soft tissues in whales (Soldevilla et al., 2005b), suggesting that there is little electron density difference between melon, blubber, muscle, and mandibular fat for live and dead specimens.

Some of the differences in each anatomic region might be a result of temperature variation during the scanning process. Because H values are calibrated based on small changes in the temperature of water, one potential source of error could result from temperature differences between specimens. The LIVE animal was removed from the water for the scanning process, so the temperature profiles might have been effected by elective circulation, as mentioned in the original study (Houser et al., 2004). Assuming the LIVE was scanned at body temperature and the FRESH and THAWED at room temperature, a 6 H unit difference is expected (Kreel and Bydder, 1979). The additional differences between the LIVE and FRESH with the THAWED values suggest alterations caused by the freezing and thawing process and/or differences between scanners.

It is noteworthy that the smallest changes in H values occurred in the tissues we know to be associated with sound propagation (melon), which is contrary to previous studies that suggested the melon in odontocetes may be particularly sensitive to postmortem effects because it contains specialized acoustic fats (Malins and Varanasi, 1975; Varanasi et al., 1975). In addition, the morphological comparisons showed little change in melon structure. The difference between the highest density in the THAWED specimens and the lowest H values in the LIVE specimen can be explained by the specific composition of the biological material. Water comprises 75% of most soft tissues, and the physical properties of the tissue are consequently dominated by its presence (Duck,

1990). Thawed postmortem specimens must be kept from dehydrating if reliable information is to be extracted using CT. Flash freezing, although not investigated in this study, might produce the most reliable results when working with frozen postmortem biological material.

In the freezing and thawing experiments, the sound speed measurements in the tissue groups (melon, connective tissue, blubber, and muscle) remained fairly constant until approximately 120 hr after death (Fig. 6). The insignificant effect on sound speed from the freezing and thawing process found in this study is consistent with the results of previous studies. Ultrasonic sound speeds through frozen and thawed tissues were compared with fresh tissues, and no significant difference was reported for the human breast (Foster et al., 1984), myocardial tissues (Dent et al., 2000), and mammalian tissues (Van der Steen et al., 1991).

The small changes in sound speed observed in all tissue types at 25 hr after death should be investigated further using a larger sample size. The measured changes might be a result of the handling process and/or loss of fluid from the tissues. The large variance in the blubber samples near the surface of the heads in this study and in that of Fitzgerald (1975) may be a result of the loss of water from the collagen fiber matrix from dehydration in the freezing process. There is also a potential for changes to happen in the first 6 hr after death before the first data points were collected for this study (Kremkau et al., 1981).

The results of this study suggest that postmortem biological material can represent live tissues both in morphology and tissue properties, but within certain limits. The limits established in this study combined with previous studies provide a framework for quantifying the viscoelastic properties of mammalian tissues that are not easily measured in vivo. Physical properties of noncontractile soft tissues have been investigated as a function of time after death. Kremkau et al. (1981) found a decrease in ultrasonic sound speed in the human brain within the first 24 hr of death, but then found sound speed to be constant thereafter. For the human lens and vitreous, no change in ultrasonic sound speed 70 hr after death was found (Jansson and Kock, 1962). Investigation into the viscoelastic properties of canine intervertebral discs, whale blubber, beef fat, and human bone, however, show a dramatic change within the first 12 hr of death (Fitzgerald, 1975; Fitzgerald and Fitzgerald, 1995). Although the response of specific tissue types and organs from postmortem effects is important, when modeling a functioning biological system, treatment of the specimens should be conservative and measurements should always be taken as soon as possible after death based on the results of this study.

Although live tissue offers the most reliable results to answer physiological questions, the results of this study support the use of postmortem CT data to extract anatomic geometry and some tissue properties. Furthermore, our results have important implications for modeling the acoustic function of cephalic tissues in odontocetes. The potential for extracting data from CT images from postmortem animals to estimate tissue properties for finite element models is promising. These modeling techniques can be used to simulate propagation of biologically relevant sounds and noise produced

in the surrounding environment and the interactions with the tissues.

Can the tissue properties measured in this study be expanded to understand additional properties? Longitudinal wave velocity is determined by the bulk modulus, rigidity modulus, and density of the tissue (Duck, 1990). Although this study did not measure the elasticity of tissues, the combined consistency of density (Fig. 5) and sound speed (Fig. 6) indicate that the bulk modulus for these tissues were conserved through each treatment. Furthermore, the mechanical properties of various connective tissues were not found to be significantly different from fresh tissue after freezing and thawing (van Brocklin and Ellis, 1965; Woo et al., 1986; Quirinia and Viidik, 1991). In contrast, Krag and Andreassen (2003) found a 20% decrease in the tensile elastic modulus of the porcine eye lens. In a study that compared the elastic shear modulus and dynamic viscosity of fresh dog vocal fold tissues to thawed tissues that were frozen at different rates, no difference for tissues that were quick frozen but significant changes for slowly frozen tissues were found (Chan and Titze, 2003). Although further analyses are needed to determine whether additional properties can be drawn from those measured in this study, the results provide a framework for future analyses.

This study supports the legitimacy of using CT data from postmortem specimens for addressing research questions investigating morphology, tissue properties, and biologically functioning tissues. At the same time, workers should be cognizant of the limits of these techniques and design experiments conservitively based on procedures presented in this study.

ACKNOWLEDGMENTS

LITERATURE CITED

Aroyan JL. 2001. Three-dimensional modeling of hearing in *Delphinus delphis*. J Acoust Soc Am 110:3305–3318.

Aroyan JL, Cranford TW, Kent J, Norris KS. 1992. Computer modeling of acoustical beam formation in *Delphinus delphis*. J Acoust Soc Am 92:2539–2545.

Au WWL. 1993. The sonar of dolphins. New York: Springer.

Au WWL, Kastelein RA, Benoit-Bird KJ, Cranford TW, McKenna MF. 2006. Acoustic radiation from the head of echolocating harbor porpoises (Phocoena phocoena). J Exp Biol 209:2726–2733.

Carpenter KE, Berra TM, Humphries JM Jr. 2004. Swim bladder and posterior lateral line nerve of the nursery fish, *Kurtus gulliveri* (Perciformes: Kurtidae). J Morphol 260:193–200.

Chan R, Titze I. 2003. Effect of postmortem changes and freezing on the viscoelastic properties of vocal fold tissues. Ann Biomed Eng 31:482–491.

Chen CT, Millero FJ. 1977. Speed of sound in seawater at high pressures. J Acoust Soc Am 62:1129–1135.

Cranford T. 1992. Functional Morphology of the odontocete forehead: implications for sound generation. In: Biology. Santa Cruz: University of California, Santa Cruz.

Cranford TW. 1996. Functional morphology and homology in the odontocete nasal complex: implications for sound generation. J Morphol 228:223–285.

Cranford T, Amundin M. 2004. Biosonar pulse production in Odontocetes. In: Thomas JA, Moss CF, Vater M, editors. Echolocation in bats and dolphins. Chicago: University of Chicago Press. p 27–35.

Cranford TW, Van Bonn WG, Chaplin JA, Carr DA, Carder AJ. 1997. Visualizing dolphin sonar signal generation using high-speed video endoscopy. J Morphol 102:3123.

Cranford TW, Elsberry WR, Blackwood JA, Carr DA, Kamolnick T, Todd M, Van Bonn WG, Carder AJ, Ridgway SH, Bozlinski DA, Decker EC. 2000. Physiological evidence for two independent sonar signal generators in the bottlenose dolphin. J Acoust Soc Am 108:2613.

Dent CL, Scott MJ, Wickline SA, Hall CS. 2000. High-frequency ultrasound for quantitative characterization of myocardial edema. Ultrasound Med Biol 26:375–384.

Duck FA. 1990. Physical properties of tissue: a comprehensive reference book. San Diego: Academic Press Ltd.

Estes J, Quist W, Lo Gerfo F, Costello P. 1998. Noninvasive characterization of plaque morphology using helical computed tomography. J Cardiovasc Surg 39:527–534.

Fitzgerald ER. 1975. Dynamic mechanical measurements during the life to death transition in animal tissues. Biorheology 12:397–408.

Fitzgerald ER, Fitzgerald JW. 1995. Blubber and compliant coatings for drag reduction in water. I. Viscoelastic properties of blubber and compliant coating materials. Mater Sci Eng C2:209–214.

Foster FS, Straban M, Austin G. 1984. The ultrasound macroscope: initial studies of breast tissue. Ultrason Imaging 6:243–261.

Heyning JE. 1989. Comparative facial anatomy of beaked whales (Ziphiidae) and a systematic revision among the families of extant Odontoceti. Contrib Sci 405:1N–64N.

Houser DS, Finneran J, Carder D, Van Bonn W, Smith C, Hoh C, Mattrey R, Ridgway SH. 2004. Structural and functional imaging of bottlenose dolphin (*Tursiops truncatus*) cranial anatomy. J Exp Biol 207:3657–3665.

Jansson F, Kock E. 1962. Determination of the velocity of ultrasound in the human lens and vitreous. Acta Ophthalmol 40:420–433.

Krag S, Andreassen T. 2003. Mechanical properties of the human lens capsule. Prog Retin Eye Res 22:749–767.

Kreel L, Bydder GM. 1979. The temperature dependence of computed tomography attenuation values. J Comput Assist Tomogr 3:506–510.

Kremkau FW, Barnes RW, McGraw CP. 1981. Ultrasonic attenuation and propagation speed in normal human brain. J Acoust Soc Am 70:29–38.

Maisano JA, Bell CJ, Gauthier J, Rowe T. 2002. Osteoderms and palpebral in *Lanthanotus borneensis* (Squamata: Anguimorpha). J Herpetol 36:678–682.

Malins D, Varanasi U. 1975. Cetacean Biosonar: Part 2: The biochemistry of lipids in acoustic tissues. In: Malins D, Sargent J, editors. Biochemical and biophysical perspectives in marine biology. New York: Academic Press. p 237–287.

Marcucci C, Nyhan D, Simon BA. 2001. Distribution of pulmonary ventilation using Xe-enhanced computed tomography in prone and supine dogs. J Appl Physiol 90:421–430.

Marino L, Meshea DW, Uhen M. 2004. Origin and evolution of large brains in toothed whales. Anat Rec 281A:1–9.

McKenna MF. 2005. Comparative morphology of the odontocete melon: functional and evolutionary interpretations. San Diego: San Diego State University Biology Department. p 211.

Mead J. 1975. Anatomy of the external nasal passages and facial complex in the Delphinidae (Mammalia: Cetacea). Smithson Contrib Zool 207.

Mull R. 1984. Mass estimates by computed tomography: physical density from CT numbers. AJR Am J Roentgenol 143:1101–1104.

Quirinia A, Viidik A. 1991. Freezing for postmortal storage influences the biomechanical properties of linear skin wounds. Biomechanics 24:819–823.

Richardson WJ, Charles R Greene J, Malme CI, Thomson DH. 1995. Marine mammals and noise. San Diego: Academic Press.

Robb RA. 1999. Biomedical imaging, visualization and analysis. New York: John Wiley and Sons.

Robb RA, Barillot C. 1989. Interactive display and analysis of 3-D medical images. IEEE Trans Med Imaging 8:217–226.

Robb RA, Hanson DP, Karwoski RA, Larson AG, Workman EL, Stacy MC. 1989. ANALYZE: a comprehensive, operator-interactive software package for multidimensional medical image display and analysis. Comput Med Imaging Graph 13:433–454.

Rommel S. 1990. Osteology of the bottlenose dolphin. In: Leatherwood S, Reeves RR, editors. The bottlenose dolphin. San Diego: Academic Press Inc. p 29–49.

Schroeder. 2001. Non-invasive characterization of coronary lesion morphology by multi-slice computed tomography: a promising new technology for risk stratification of patients with coronary artery disease. Heart 85:567–578.

Soldevilla MS, McKenna ME, Wiggins SM, Shadwick RE, Cranford TW, Hildebrand JA. 2005a. Cuvier's beaked whale (Ziphius cavirostris) head tissues: physical properties and CT imaging. J Exp Biol 208:2319–2332.

Soldevilla MS, McKenna MF, Wiggins SM, Shadwick RE, Cranford TW, Hildebrand JA. 2005b. Cuvier's beaked whale (Ziphius cavirostris) head tissues: physical properties and CT imaging. J Exp Biol 208:2319–2332.

SPSS Statistical Software. 2000. 10th ed. Chicago: SPSS Inc.

Stern E, Webb W. 1993. Dynamic imaging of lung morphology with ultrafast high-resolution computed tomography. J Thorac Imaging 8:273–282.

Summers AP, Ketcham RA, Rowe T. 2004. Structure and function of the horn shark (Heterodontus francisci) cranium through ontogeny: development of a hard prey specialist. J Morphol 260:1–12.

Terheyden H, Maune S, Mertens J, Hilberg O. 2000. Acoustic rhinometry: validation by three-dimensionally reconstructed computer tomographic scans. J Appl Physiol 89:1013–1021.

van Brocklin JD, Ellis DG. 1965. A study of the mechanical behavior of toe extensors tendons under applied stress. Arch Phys Med Rehabil 46:369–373.

Van der Steen AFW, Cuypers MHM, Thijssen JM, de Wilde PCM. 1991. Influence of histochemical preparation on acoustic parameters of liver tissue: a 5-MHz study. Ultrasound Med Biol 17:879–891.

Varanasi U, Feldman H, Malins D. 1975. Molecular basis for formation of lipid sound lens in echolocating cetaceans. Nature 255:340–343.

Woo SL, Orlando CA, Camp JF, Akeson WH. 1986. Effects of postmortem storage by freezing on ligament tensile behavior. J Biomech 19:399–404.